Electronic Supplementary Material (ESI) for Physical Chemistry Chemical Physics.

Kinetics of contracting geometry-type reactions in the solid state: Implications from the thermally induced transformation processes of α-oxalic acid dihydrate

Satoki Kodani and Nobuyoshi Koga*

Department of Science Education, Graduate School of Education, Hiroshima University, 1-1-1 Kagamiyama, Higashi-Hiroshima 739-8524, Japan

Contents

* Corresponding author. E-mail: nkoga@hiroshima-u.ac.jp

S1. Sample characterization

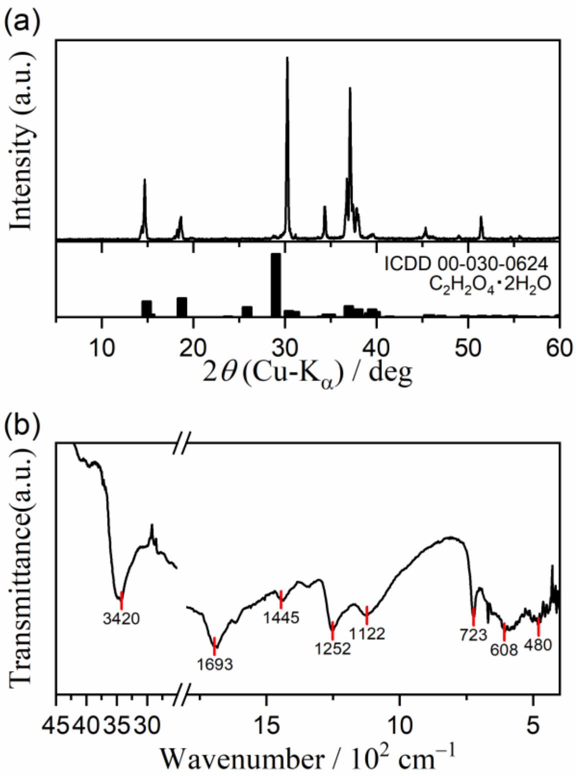

Figure S1. (a) XRD pattern and (b) FT-IR spectrum of the CPs sample.

Table S1. Assignments of IR absorption peaks[38-40]

Peak/cm^{-1}	Vibration mode
3420	OH stretching
1693	Stretching of the C=O moiety of the carboxyl groups
1445	H–O–H bending
1252	C–O stretching
1122	out-of-plane vibration of the hydroxyl group of oxalic acid
723	Combination band
608	Out of plane vibration that involve five atoms
480	Combination band

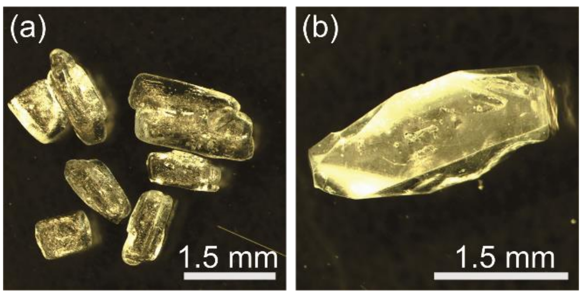

Figure S2. Optical microscopic views of the samples: (a) CPs and (b) SC samples.

S2. Overall thermal behavior

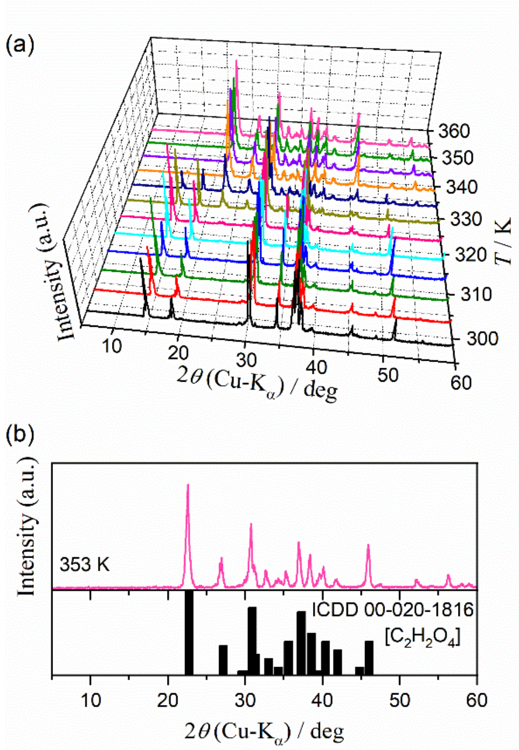

Figure S3. (a) Changes in the XRD pattern of the CPs sample during a stepwise isothermal heating from room temperature to 353 K in steps of 5 K under a dynamic flow of dry N_2 gas and (b) the diffraction pattern of the product solid at 353 K.

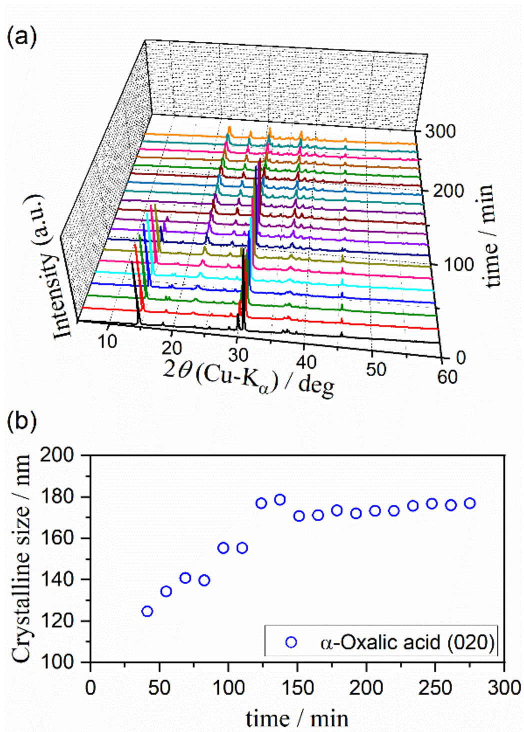

Figure S4. (a) Changes in the XRD pattern of the CPs sample during isothermal heating at 323 K under a dynamic flow of dry N_2 gas and (b) changes in the crystallite size of the solid product, i.e., α-oxalic acid anhydride, calculated with reference to (020) diffraction peak.

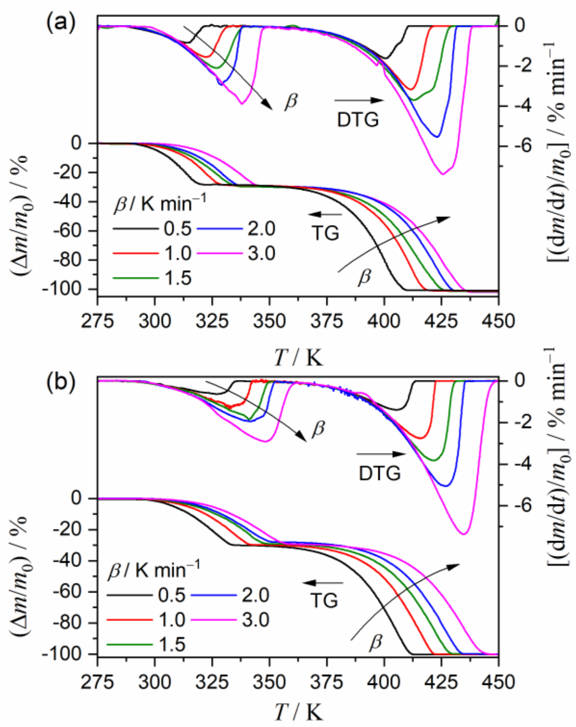

Figure S5. TG–DTG curves for the samples at various β values under a dynamic flow of dry N_2 gas: (a) CPs (m_0 = 3.09 ± 0.19 mg) and (b) SC (m_0 = 3.32 ± 0.17 mg) samples.

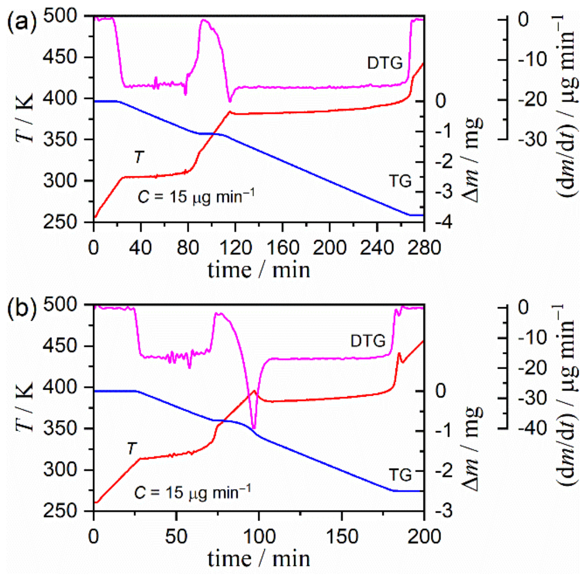

Figure S6. Typical T–TG–DTG records for the samples recorded using the CRTA mode at a C of 15 μg min^{-1} under a dynamic flow of dry N_2 gas: (a) CPs (m_0: 3.71 mg) and (b) SC (m_0: 2.55 mg) samples.

S3. Thermal dehydration process

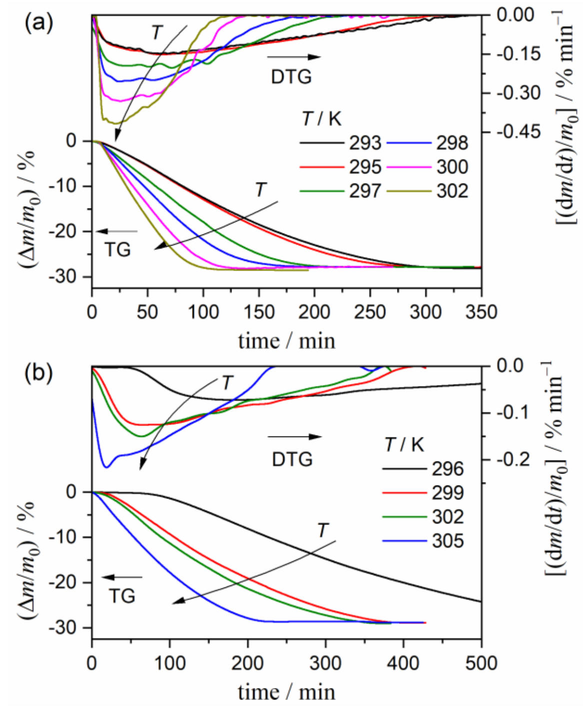

Figure S7. Typical TG–DTG curves for the thermal dehydration of the dihydrate to form anhydride recorded under isothermal conditions at various T: (a) CPs (m_0 = 3.59 ± 0.13 mg) and (b) SC (m_0 = 3.11 ± 0.28 mg). Time zero was defined as the time at which the sample temperature reached to the programmed temperature for isothermal measurement.

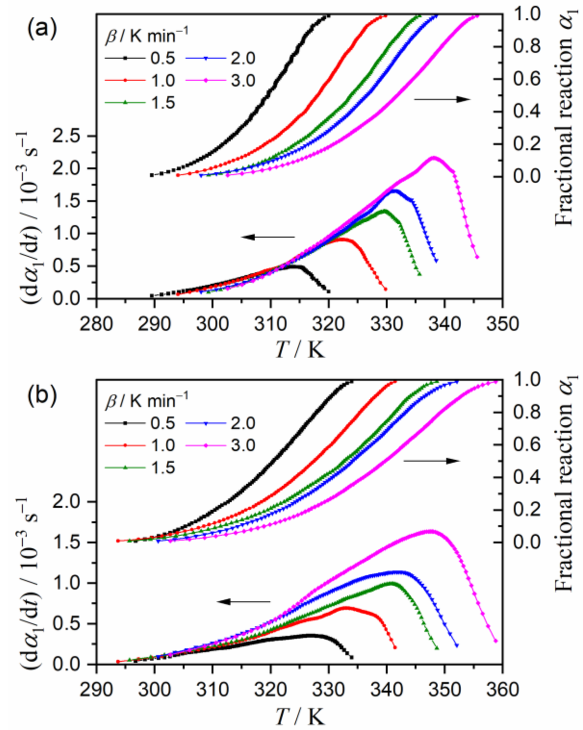

Figure S8. Kinetic curves for the thermal dehydration recorded under linear nonisothermal conditions at various β values: (a) CPs and (b) SC samples.

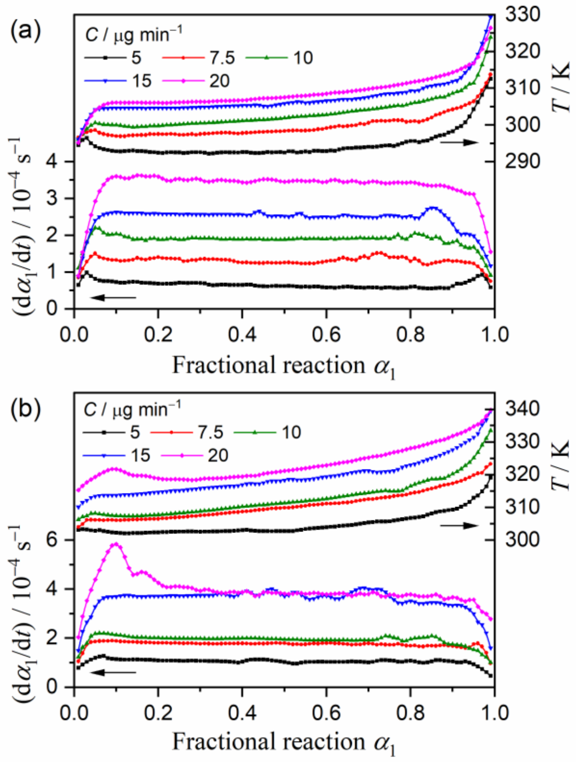

Figure S9. Kinetic curves for the thermal dehydration recorded under CR conditions at various C values: (a) CPs and (b) SC samples.

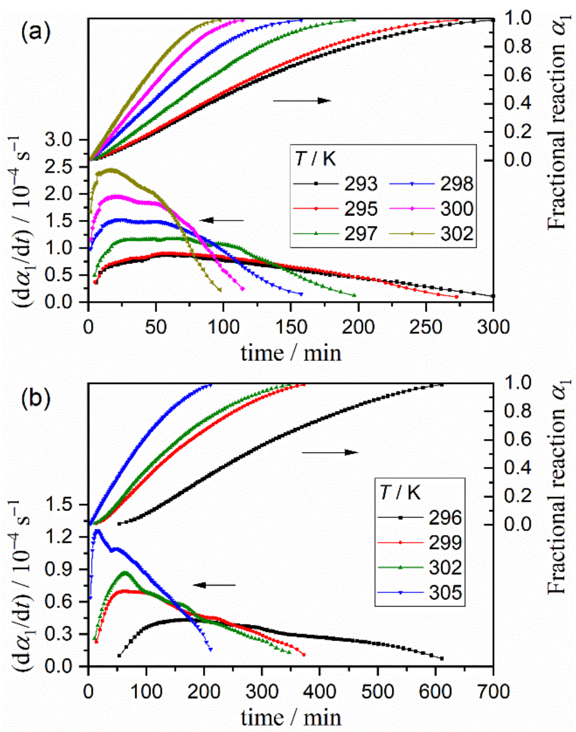

Figure S10. Kinetic curves for the thermal dehydration recorded under isothermal conditions at various T values: (a) CPs and (b) SC samples.

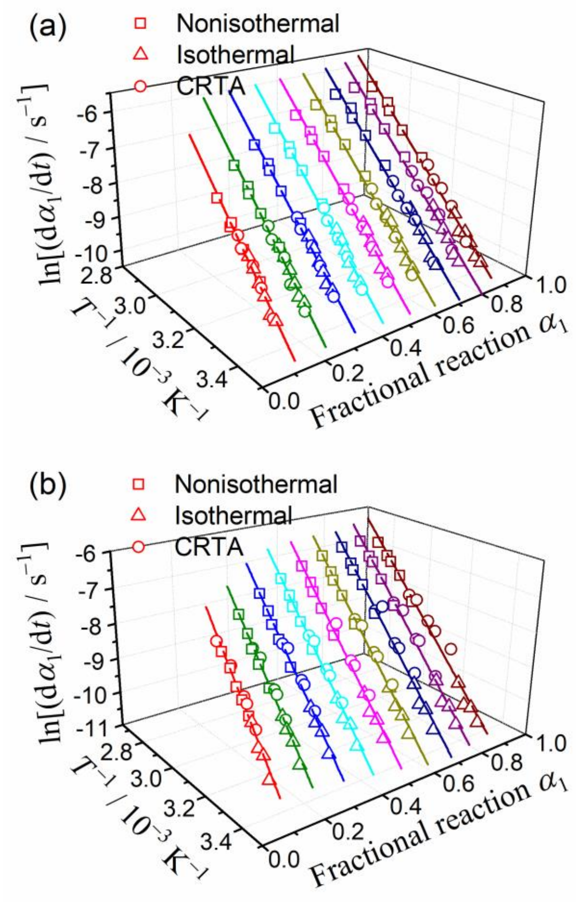

Figure S11. Friedman plots for the mass-loss process of the thermal dehydration at various α_1 from 0.1 to 0.9 in steps of 0.1: (a) CPs and (b) SC samples.

Table S2. Differential kinetic equations of the SR–PBR(n) models

n		$\frac{\mathrm{d}\alpha}{\mathrm{d}t} =$
1	a) $t \leq 1/k_{\mathrm{PBR(1)}}$:	$k_{\mathrm{PBR(1)}}[1-\exp(-k_{\mathrm{SR}}t)]$
	b) $t \geq 1/k_{\mathrm{PBR(1)}}$:	$k_{\mathrm{PBR(1)}}\exp(-k_{\mathrm{SR}}t)\left[\exp\left(\frac{k_{\mathrm{SR}}}{k_{\mathrm{PBR(1)}}}\right)-1\right]$
2	a) $t \leq 1/k_{\mathrm{PBR(2)}}$:	$-2k_{\mathrm{PBR(2)}}\left[\left(1+\frac{k_{\mathrm{PBR(2)}}}{k_{\mathrm{SR}}}\right)\exp(-k_{\mathrm{SR}}t)+k_{\mathrm{PBR(2)}}t-\left(1+\frac{k_{\mathrm{PBR(2)}}}{k_{\mathrm{SR}}}\right)\right]$
	b) $t \geq 1/k_{\mathrm{PBR(2)}}$:	$-2k_{\mathrm{PBR(2)}}\exp(-k_{\mathrm{SR}}t)\left[1+\frac{k_{\mathrm{PBR(2)}}}{k_{\mathrm{SR}}}-\frac{k_{\mathrm{PBR(2)}}}{k_{\mathrm{SR}}}\exp\left(\frac{k_{\mathrm{SR}}}{k_{\mathrm{PBR(2)}}}\right)\right]$
3	a) $t \leq 1/k_{\mathrm{PBR(3)}}$:	$-3k_{\mathrm{PBR(3)}}\left[\left(1+2\frac{k_{\mathrm{PBR(3)}}}{k_{\mathrm{SR}}}+2\left(\frac{k_{\mathrm{PBR(3)}}}{k_{\mathrm{SR}}}\right)^2\right)\exp(-k_{\mathrm{SR}}t)-\left(-k_{\mathrm{PBR(3)}}t\right)^2 + 2k_{\mathrm{PBR(3)}}\left(\frac{k_{\mathrm{PBR(3)}}}{k_{\mathrm{SR}}}+1\right)t-\left(1+2\frac{k_{\mathrm{PBR(3)}}}{k_{\mathrm{SR}}}+2\left(\frac{k_{\mathrm{PBR(3)}}}{k_{\mathrm{SR}}}\right)^2\right)\right]$
	b) $t \geq 1/k_{\mathrm{PBR(3)}}$:	$3k_{\mathrm{PBR(3)}}\exp(-k_{\mathrm{SR}}t)\left[2\left(\frac{k_{\mathrm{PBR(3)}}}{k_{\mathrm{SR}}}\right)^2\left(\exp\left(\frac{k_{\mathrm{SR}}}{k_{\mathrm{PBR(3)}}}\right)-1\right)-\left(1+2\frac{k_{\mathrm{PBR(3)}}}{k_{\mathrm{SR}}}\right)\right]$

Table S3. Optimized k_{SR} and $k_{\mathrm{PBR(2)}}$ for the thermal dehydration of α-oxalic acid dihydrate at various temperatures

Sample	T / K	k_{SR} / s^{-1}	$k_{\mathrm{PBR(2)}}$ / s^{-1}	$R^{2,\,a}$	
				differential	integral
CPs	292.8	7.92×10^{-4}	5.26×10^{-5}	0.9970	0.9998
	294.7	6.88×10^{-4}	5.89×10^{-5}	0.9939	0.9997
	296.8	1.01×10^{-3}	8.11×10^{-5}	0.9868	0.9990
	298.4	1.19×10^{-3}	1.04×10^{-4}	0.9932	0.9998
	300.5	1.35×10^{-3}	1.36×10^{-4}	0.9905	0.9989
	300.9	1.15×10^{-3}	1.77×10^{-4}	0.9872	0.9957
SC	296.1	3.43×10^{-4}	2.60×10^{-5}	0.9966	0.9992
	299.0	1.03×10^{-3}	3.95×10^{-5}	0.9985	0.9993
	302.0	1.48×10^{-3}	4.40×10^{-5}	0.9764	0.9990
	305.0	5.82×10^{-3}	6.54×10^{-5}	0.9984	0.9991

[a] determination coefficient of the nonlinear least squares analysis.

S4. Sublimation/decomposition process

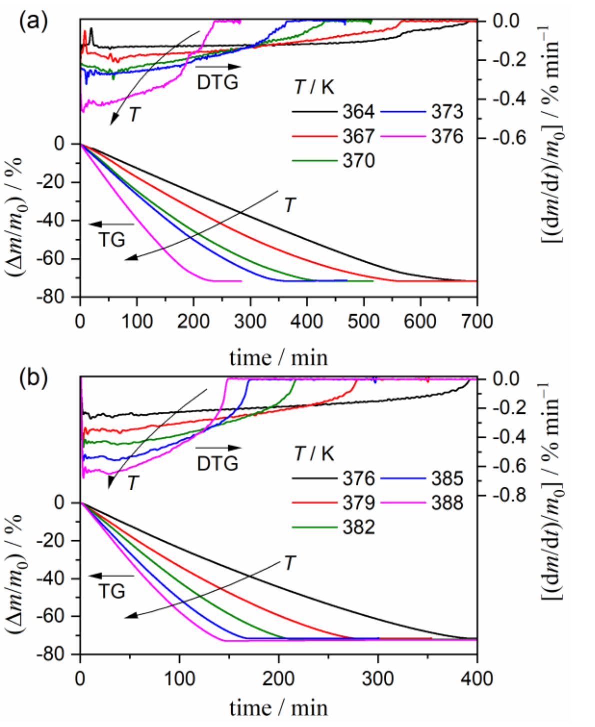

Figure S12. TG–DTG curves for the thermally induced sublimation/decomposition of the anhydrous oxalic acid produced by the thermal dehydration of the dihydrate, as recorded under isothermal conditions at various T: (a) CPs (m_0 = 3.57± 0.09 mg) and (b) SC (m_0 = 2.98 ± 0.12 mg) samples. Time zero was defined as the time at which the sample temperature reached to the programmed temperature for isothermal measurement.

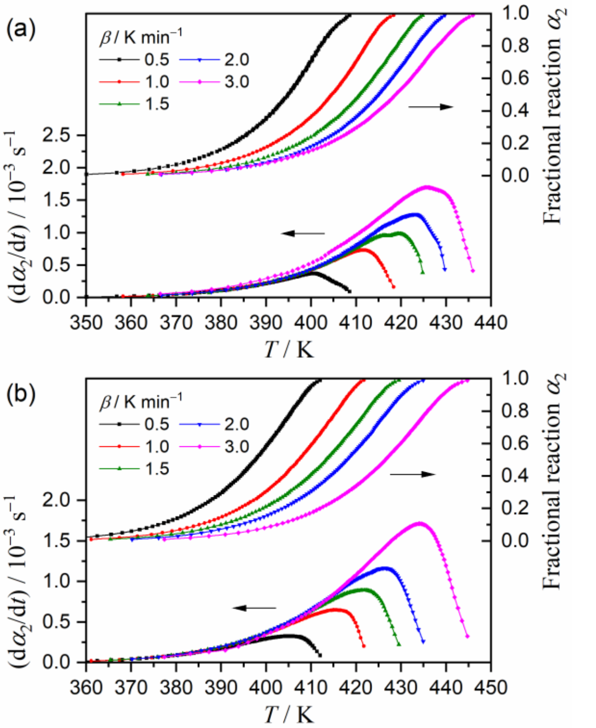

Figure S13. Kinetic curves for the thermally induced sublimation/decomposition of the anhydrous oxalic acid produced by the thermal dehydration of the dihydrate recorded under linear nonisothermal conditions at various β values: (a) CPs and (b) SC samples.

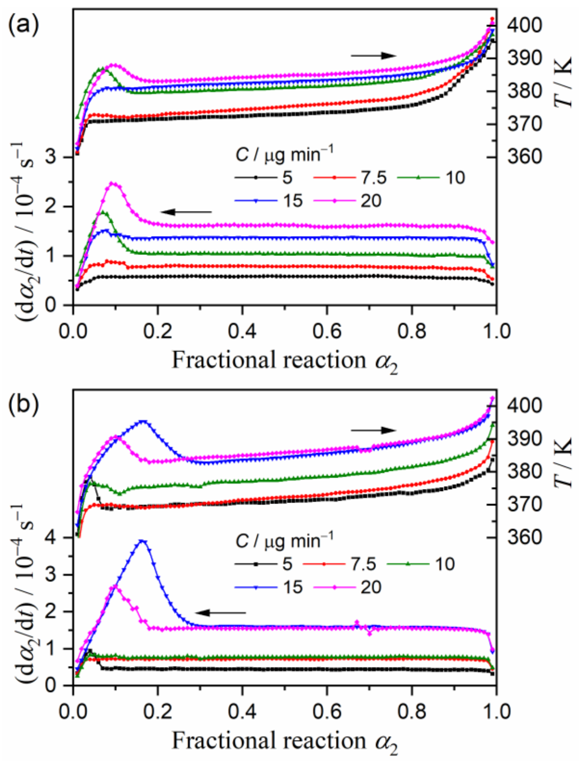

Figure S14. Kinetic curves for the thermally induced sublimation/decomposition of the anhydrous oxalic acid produced by the thermal dehydration of the dihydrate recorded under CR conditions at various C values: (a) CPs and (b) SC samples.

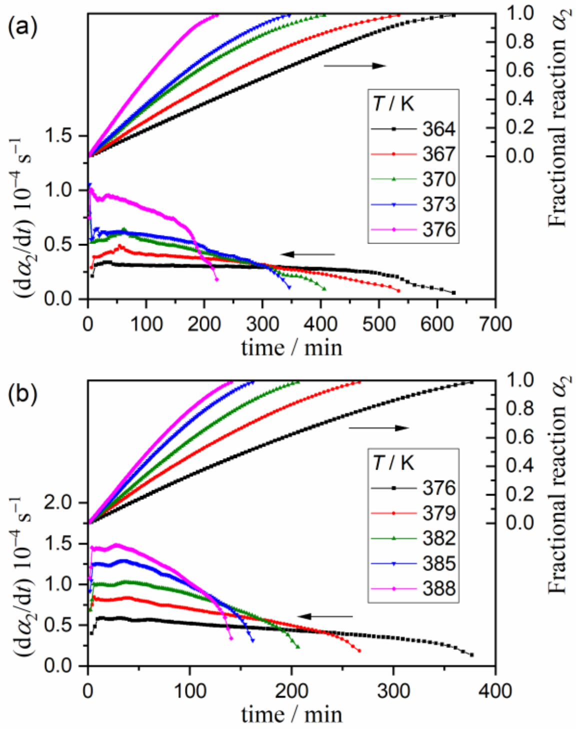

Figure S15. Kinetic curves for the thermally induced sublimation/decomposition of the anhydrous oxalic acid produced by the thermal dehydration of the dihydrate recorded under isothermal conditions at various T values: (a) CPs and (b) SC samples.

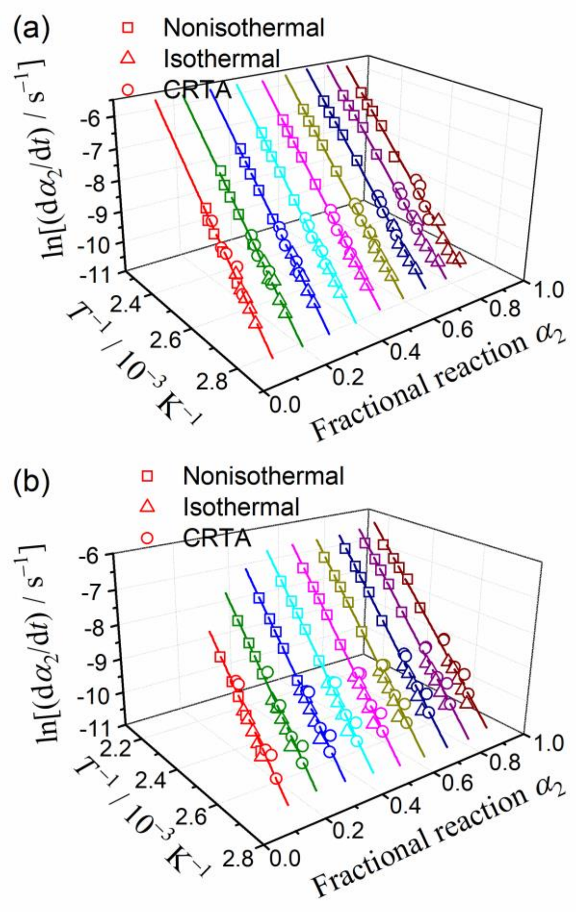

Figure S16. Friedman plots for the mass-loss process of the thermally induced sublimation/decomposition of the anhydrous oxalic acid produced by the thermal dehydration of the dihydrate at various α_2 from 0.1 to 0.9 in steps of 0.1: (a) CPs and (b) SC samples.